in Proc. IEEE GLOBECOM 2000
San Francisco (CA), Nov. 2000.

PREDICTIVE EQUALIZATION OF TIME-VARYING CHANNELS FOR CODED OFDM/BFDM SYSTEMS

Dieter Schafhuber, Gerald Matz, and Franz Hlawatsch

Institute of Communications and Radio-Frequency Engineering, Vienna University of Technology
Gusshausstrasse 25/389, A-1040 Vienna, Austria
phone: +43 1 58801 38916, fax: +43 1 58801 38999, email: gmatz@aurora.nt.tuwien.ac.at
web: http://www.nt.tuwien.ac.at/dspgroup/time.html

ABSTRACT

We propose a novel receiver for coded *orthogonal/biorthogonal frequency division multiplexing* (OFDM/BFDM) communications over time-varying mobile radio channels. The receiver uses decision-directed predictive equalization and thus does not require regular transmission of pilot symbols. An optimum channel predictor and its efficient implementation are discussed, and simulation results are presented.

1. INTRODUCTION

Orthogonal frequency division multiplexing (OFDM) is an attractive modulation technique for high data-rate communications [1–4]. Traditional OFDM systems employ rectangular transmit/receive filters that are orthogonal when translated in time and frequency. However, *biorthogonal frequency division multiplexing* (BFDM) systems employing biorthogonal transmit and receive filters were recently recognized to have improved properties regarding intersymbol interference (ISI) and interchannel interference (ICI) [5, 6].

Here, we propose an OFDM/BFDM receiver for random time-varying channels that employs decision-directed linear channel prediction. Regular transmission of pilot symbols for channel estimation [7, 8] is not required.

This paper is organized as follows. Section 2 reviews coded OFDM/BFDM communication over time-varying channels. The structure of the novel receiver is described in Section 3. The design of the channel predictor is discussed in Sections 4 and 5. Finally, simulation results are presented in Section 6.

2. OFDM/BFDM SYSTEM MODEL

OFDM/BFDM system. The baseband version of a coded OFDM/BFDM communication system is depicted in Fig. 1. At the transmitter/modulator, N bits $b_{n,l}$ ($l = 0, \ldots, N-1$) are block-coded and mapped onto K transmit symbols $a_{n,k}$ ($n \in \mathbb{Z}$ is the time index, $k \in \{0, \ldots, K-1\}$ is the subcarrier index). The transmit signal is given by

$$s(t) \;=\; \sum_{n=-\infty}^{\infty} \sum_{k=0}^{K-1} a_{n,k}\, g_{n,k}(t)\,.$$

Here, the functions $g_{n,k}(t) \triangleq g(t-nT)\, e^{j2\pi kF(t-nT)}$ are time-frequency translates of a transmit pulse $g(t)$, with T and F denoting the symbol duration and subcarrier frequency spacing, respectively. The received signal is[1]

$$r(t) \;=\; (\mathbb{H}\, s)(t) + w(t) \;=\; \int_{\tau} h(t,\tau)\, s(t-\tau)\, d\tau + w(t)\,,$$

where $h(t,\tau)$ is the impulse response of the time-varying channel $\mathbb{H}$ [9, 10] and $w(t)$ is zero-mean stationary white noise (with power spectral density N_0) that is uncorrelated with the transmit symbols $a_{n,k}$. From the received signal $r(t)$, the demodulator derives K sequences $x_{n,k}$ according to

$$x_{n,k} \;=\; \langle r, \gamma_{n,k} \rangle \;=\; \int_t r(t)\, \gamma_{n,k}^*(t)\, dt\,, \qquad k = 0, \ldots, K-1\,,$$

where $\gamma_{n,k}(t) \triangleq \gamma(t-nT)\, e^{j2\pi kF(t-nT)}$ with some receive pulse $\gamma(t)$. The sequences $x_{n,k}$ are then further processed to yield estimates $\hat{b}_{n,l}$ of the bits $b_{n,l}$ (see Section 3). For a conventional OFDM system, $g(t) = \frac{1}{\sqrt{T_0}} \mathrm{rect}_T(t + T_{\mathrm{CP}})$ and $\gamma(t) = \frac{1}{\sqrt{T_0}} \mathrm{rect}_{T_0}(t)$, where $\mathrm{rect}_{t_0}(t)$ equals 1 for $0 \le t < t_0$ and 0 otherwise. Here, T_0 is the duration of $\gamma(t)$, T_{CP} is the duration of the *cyclic prefix*, the symbol duration is given by $T = T_0 + T_{\mathrm{CP}}$, and the subcarrier spacing equals $F = 1/T_0$ [3, 4].

One easily shows the input-output relation [5]

$$x_{n,k} \;=\; \sum_{n'=-\infty}^{\infty} \sum_{k'=0}^{K-1} q_{n,k,n',k'}\, a_{n',k'} \;+\; z_{n,k}\,, \qquad (1)$$

with $q_{n,k,n',k'} = \langle \mathbb{H}\, g_{n',k'}, \gamma_{n,k} \rangle$ and $z_{n,k} = \langle w, \gamma_{n,k} \rangle$. For $n \neq n'$ and $k \neq k'$, the coefficients $q_{n,k,n',k'}$ describe the ISI and ICI introduced by the channel $\mathbb{H}$. The noise term $z_{n,k}$ has correlation (note that E denotes expectation)

$$\mathrm{E}\left\{ z_{n,k}\, z_{n-m,k-l}^* \right\} \;=\; N_0\, e^{j2\pi TF(k-l)m}\, \langle \gamma, \gamma_{m,l} \rangle\,. \qquad (2)$$

The $z_{n,k}$ are white (uncorrelated) if and only if the $\gamma_{n,k}(t)$ are orthogonal, which is the case in an OFDM system.

In the case of an ideal channel defined by $\mathbb{H} = \mathbb{I}$ and $N_0 = 0$, we have perfect demodulation (i.e., $x_{n,k} = a_{n,k}$) if and only if the transmit/receive pulses satisfy the (bi)orthogonality condition $\langle g_{n',k'}, \gamma_{n,k} \rangle = \delta_{n-n'} \delta_{k-k'}$.

Approximate system relation. In what follows, we assume that the channel $\mathbb{H}$ is *underspread* [5, 11, 12], i.e., it introduces only small delays and/or Doppler shifts, and that the transmit/receive pulses are well concentrated in time and frequency (note, however, that the frequency concentration of conventional OFDM pulses is only moderate). In that case, it can be shown that the ISI/ICI terms in (1) approximately

Funding by FWF grant P11904-TEC.

[1] Unless stated otherwise, integrals are from $-\infty$ to ∞.

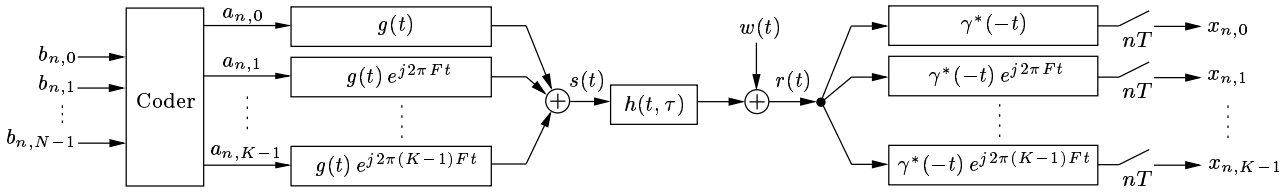

Figure 1: *Model for OFDM/BFDM communication over a time-varying channel.*

vanish, i.e., $q_{n,k,n',k'} \approx 0$ for $n \neq n'$, $k \neq k'$ [5, 12]. Relation (1) then simplifies to

$$x_{n,k} \;\approx\; H_{n,k}\, a_{n,k} + z_{n,k}\,, \tag{3}$$

where $H_{n,k} = q_{n,k,n,k} \approx L_{\mathbb{H}}(nT, kF)$ with the *time-varying transfer function* [9–12]

$$L_{\mathbb{H}}(t,f) \;\triangleq\; \int_{\tau} h(t,\tau)\, e^{-j2\pi f\tau}\, d\tau\,. \tag{4}$$

Statistical channel characterization. In what follows, the time-varying channel $\mathbb{H}$ will be assumed to be random. Specifically, we assume that $\mathbb{H}$ is *wide-sense stationary with uncorrelated scatterers* (WSSUS) [9, 10] as well as uncorrelated with the transmit symbols $a_{n,k}$ and the noise $w(t)$. Due to the WSSUS assumption, the time-varying transfer function $L_{\mathbb{H}}(t,f)$ in (4) is a 2-D stationary random process with *time-frequency correlation function* [9, 10]

$$R_{\mathbb{H}}(t',f') \;\triangleq\; \mathrm{E}\left\{L_{\mathbb{H}}(t,f)\, L^*_{\mathbb{H}}(t-t', f-f')\right\}\,.$$

The correlation function of $H_{n,k}$ can be approximated as

$$R_H[m,l] \;\triangleq\; \mathrm{E}\left\{H_{n,k} H^*_{n-m,k-l}\right\} \;\approx\; R_{\mathbb{H}}(mT, lF)\,, \tag{5}$$

since $H_{n,k} \approx L_{\mathbb{H}}(nT, kF)$. An alternative second-order statistic of the channel is the *scattering function* [9, 10]

$$S_{\mathbb{H}}(\tau,\nu) \;=\; \int_{t'}\int_{f'} R_{\mathbb{H}}(t',f')\, e^{-j2\pi(\nu t' - \tau f')}\, dt'\, df'\,. \tag{6}$$

The function $R_H[m,l]$ (or, equivalently, $S_{\mathbb{H}}(\tau,\nu)$) constitutes the prior knowledge used for the design of the channel predictors in Sections 4 and 5. Its estimation is discussed e.g. in [13].

3. OFDM/BFDM RECEIVER WITH PREDICTIVE EQUALIZER

Fig. 2 shows a block diagram of the proposed receiver. The upper branch is a conventional OFDM/BFDM receiver with equalizer. Based on the approximate input-output relation (3), the received vector $\mathbf{x}_n = [x_{n,0}\,\cdots\,x_{n,K-1}]^T$ (the superscript ^{T} denotes transposition) is first equalized according to [4]

$$\alpha_{n,k} \;=\; x_{n,k}\,\frac{\widehat{H}^*_{n,k}}{|\widehat{H}_{n,k}|^2 + \sigma_z^2}\,, \qquad k = 0,\ldots,K-1\,.$$

Here, the $\widehat{H}_{n,k}$ are channel estimates (whose calculation is described below) and $\sigma_z^2 = \mathrm{E}\left\{|z_{n,k}|^2\right\} = N_0\,\|\gamma\|^2$ (cf. (2)). The equalized sequence $\boldsymbol{\alpha}_n = [\alpha_{n,0}\,\cdots\,\alpha_{n,K-1}]^T$ is then passed through a slicer and a decoder to obtain the (error-corrected) bits $\hat{\mathbf{b}}_n = [\hat{b}_{n,0}\,\cdots\,\hat{b}_{n,N-1}]^T$.

The lower branch of the receiver in Fig. 2 produces estimates $\widehat{\mathbf{H}}_{n+1} = [\widehat{H}_{n+1,0}\,\cdots\,\widehat{H}_{n+1,K-1}]^T$ of the channel weights $H_{n+1,k}$, to be used for equalization in the subsequent symbol interval (hence the delay by T in Fig. 2). The central part of the lower branch is a linear, FIR, multi-input multi-output (MIMO) predictor of length L. The predictor's input-output relation reads

$$\widehat{\mathbf{H}}_{n+1} \;=\; \sum_{m=0}^{L-1} \mathbf{C}_{n,m}\mathbf{x}_{n-m} \;=\; \boldsymbol{\mathcal{C}}_n \boldsymbol{\mathcal{X}}_n\,, \tag{7}$$

with the $K\times K$ coefficient matrices $\mathbf{C}_{n,m}$ $(m = 0,\ldots,L-1)$, the $K\times KL$ matrix $\boldsymbol{\mathcal{C}}_n = [\mathbf{C}_{n,0}\,\cdots\,\mathbf{C}_{n,L-1}]$, and the vector $\boldsymbol{\mathcal{X}}_n = [\mathbf{x}_n^T\,\cdots\,\mathbf{x}_{n-L+1}^T]^T$ of size KL. As we will see, calculation of the optimum $\mathbf{C}_{n,m}$ requires knowledge of the symbols $\mathbf{a}_n = [a_{n,0}\,\cdots\,a_{n,K-1}]^T$. To avoid transmission of pilot symbols, we adopt a decision-directed mode using estimated symbols $\hat{\mathbf{a}}_n = [\hat{a}_{n,0}\,\cdots\,\hat{a}_{n,K-1}]^T$ that are obtained by coding the error-corrected detected bits $\hat{\mathbf{b}}_n$ (see Fig. 2). Note that $\hat{\mathbf{a}}_n = \mathbf{a}_n$ only if all bit errors were corrected; otherwise, error propagation will result (see Section 6).

4. LMMSE CHANNEL PREDICTOR

We now calculate the FIR predictor that is optimum under a linear minimum mean square error (LMMSE) criterion and under the assumption of given (known) symbols, i.e., $\hat{a}_{n,k} = a_{n,k}$. We will see that the LMMSE predictor is impractical due to its high complexity. However, based on its structure a simplified predictor will be developed in Section 5.

Assuming that (3) holds exactly, the received vector can be written as

$$\mathbf{x}_n \;=\; \mathbf{A}_n\mathbf{H}_n + \mathbf{z}_n\,, \tag{8}$$

with the symbol matrix $\mathbf{A}_n = \mathrm{diag}\{a_{n,0},\ldots,a_{n,K-1}\}$, the channel vector $\mathbf{H}_n = [H_{n,0}\,\cdots\,H_{n,K-1}]^T$, and the noise vector $\mathbf{z}_n = [z_{n,0}\,\cdots\,z_{n,K-1}]^T$. Whereas $\mathbf{H}_n$ and $\mathbf{z}_n$ are stationary vector processes (note that $\mathbf{H}_n$ is stationary due to the WSSUS assumption), $\mathbf{x}_n$ is generally nonstationary due to the factor $\mathbf{A}_n$ in (8). Thus, in general, the LMMSE predictor will be a *time-varying* MIMO system.

By definition, the optimum predictor coefficient matrices $\mathbf{C}^{\mathrm{opt}}_{n,m}$ minimize the mean square error (MSE) $\epsilon[n] = \frac{1}{K}\,\mathrm{E}\left\{\|\mathbf{e}_{n+1}\|^2\right\}$ of the prediction error vector $\mathbf{e}_{n+1} = \mathbf{H}_{n+1} - \widehat{\mathbf{H}}_{n+1}$. Invoking the orthogonality principle of LMMSE estimation [14], i.e., $\mathrm{E}\left\{\mathbf{e}_{n+1}\mathbf{x}^H_{n-m}\right\} = \mathbf{0}$ for $n \in \mathbb{Z}$, $m = 0,\ldots,L-1$

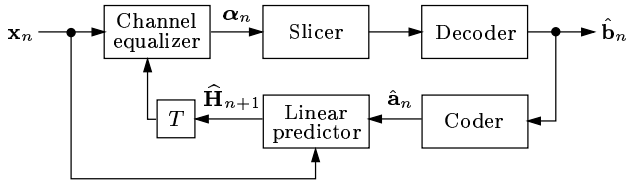

Figure 2: *OFDM/BFDM receiver with predictive equalizer.*

(the superscript ^{H} denotes Hermitian transposition), and inserting (7) and (8), we obtain the equations

$$\sum_{m'=0}^{L-1} \mathbf{C}_{n,m'}^{\text{opt}} \mathbf{A}_{n-m'} \big(\mathbf{R}_H[m-m'] + \mathbf{A}_{n-m'}^{-1} \mathbf{R}_z[m-m'] \mathbf{A}_{n-m}^{-H} \big) = \mathbf{R}_H[m+1], \qquad n \in \mathbb{Z},\ m = 0, \ldots, L-1\,. \tag{9}$$

Here, $\mathbf{R}_H[m] = \mathrm{E}\{\mathbf{H}_n \mathbf{H}_{n-m}^H\}$ denotes time-frequency channel correlation matrices with (k,l)th entry $\big(\mathbf{R}_H[m]\big)_{k,l} = R_H[m, k-l]$ (cf. (5)), and $\mathbf{R}_z[m] = \mathrm{E}\{\mathbf{z}_n \mathbf{z}_{n-m}^H\}$ is the noise correlation matrix. Introducing the block matrices

$$\boldsymbol{\mathcal{V}}_H = \big[\mathbf{R}_H[1] \cdots \mathbf{R}_H[L]\big],$$
$$\boldsymbol{\mathcal{A}}_n = \mathrm{diag}\{\mathbf{A}_n, \ldots, \mathbf{A}_{n-L+1}\},$$
$$\boldsymbol{\mathcal{R}}_H = \begin{bmatrix} \mathbf{R}_H[0] & \cdots & \mathbf{R}_H[L-1] \\ \vdots & \ddots & \vdots \\ \mathbf{R}_H[-L+1] & \cdots & \mathbf{R}_H[0] \end{bmatrix},$$
$$\boldsymbol{\mathcal{R}}_z = \begin{bmatrix} \mathbf{R}_z[0] & \cdots & \mathbf{R}_z[L-1] \\ \vdots & \ddots & \vdots \\ \mathbf{R}_z[-L+1] & \cdots & \mathbf{R}_z[0] \end{bmatrix},$$

and recalling the definition of $\boldsymbol{\mathcal{C}}_n$ in Section 3 (cf. (7)), the equations in (9) can be compactly written as

$$\boldsymbol{\mathcal{C}}_n^{\text{opt}} \boldsymbol{\mathcal{A}}_n \big(\boldsymbol{\mathcal{R}}_H + \boldsymbol{\mathcal{A}}_n^{-1} \boldsymbol{\mathcal{R}}_z \boldsymbol{\mathcal{A}}_n^{-H} \big) = \boldsymbol{\mathcal{V}}_H\,.$$

This is solved by

$$\boldsymbol{\mathcal{C}}_n^{\text{opt}} = \boldsymbol{\mathcal{W}}_n \boldsymbol{\mathcal{A}}_n^{-1}\,, \tag{10}$$

with

$$\boldsymbol{\mathcal{W}}_n = \boldsymbol{\mathcal{V}}_H \big(\boldsymbol{\mathcal{R}}_H + \boldsymbol{\mathcal{A}}_n^{-1} \boldsymbol{\mathcal{R}}_z \boldsymbol{\mathcal{A}}_n^{-H} \big)^{-1}. \tag{11}$$

Inserting in (7), and writing $\boldsymbol{\mathcal{W}}_n = [\mathbf{W}_{n,0} \cdots \mathbf{W}_{n,L-1}]$, the predictor's input-output relation is obtained as

$$\widehat{\mathbf{H}}_{n+1} = \boldsymbol{\mathcal{W}}_n \boldsymbol{\mathcal{Y}}_n = \sum_{m=0}^{L-1} \mathbf{W}_{n,m}\, \mathbf{y}_{n-m}\,. \tag{12}$$

Here,

$$\boldsymbol{\mathcal{Y}}_n \triangleq \boldsymbol{\mathcal{A}}_n^{-1} \boldsymbol{\mathcal{X}}_n = [\mathbf{y}_n^T \cdots \mathbf{y}_{n-L+1}^T]^T\,, \tag{13}$$

where

$$\mathbf{y}_n = \mathbf{A}_n^{-1} \mathbf{x}_n = [y_{n,0} \cdots y_{n,K-1}]^T \quad \text{with } y_{n,k} = \frac{x_{n,k}}{a_{n,k}}\,. \tag{14}$$

Thus, the LMMSE predictor first calculates $\boldsymbol{\mathcal{Y}}_n = \boldsymbol{\mathcal{A}}_n^{-1} \boldsymbol{\mathcal{X}}_n$, corresponding to $y_{n,k} = x_{n,k}/a_{n,k}$. For practical operation, the transmit symbols $a_{n,k}$ are replaced by estimates $\hat{a}_{n,k}$ (see Fig. 2). We note that the minimum MSE achieved by $\boldsymbol{\mathcal{C}}_n^{\text{opt}}$ is $\epsilon_{\min}[n] = R_H[0,0] - \frac{1}{K}\mathrm{tr}\{\boldsymbol{\mathcal{W}}_n \boldsymbol{\mathcal{V}}_H^H\}$, where tr denotes trace.

According to (10) and (11), calculation of $\boldsymbol{\mathcal{C}}_n^{\text{opt}}$ generally requires on-line inversion of the time-varying $KL \times KL$ matrix $\boldsymbol{\mathcal{R}}_H + \boldsymbol{\mathcal{A}}_n^{-1} \boldsymbol{\mathcal{R}}_z \boldsymbol{\mathcal{A}}_n^{-H}$ in each symbol interval, which is impractical. In Section 5, we will present a simplification of the LMMSE predictor resulting in a time-invariant system.

Special case. The on-line matrix inversion is avoided if the transmit symbols $a_{n,k}$ are drawn from a PSK alphabet and if $z_{n,k}$ is white (i.e., $\boldsymbol{\mathcal{R}}_z = \sigma_z^2 \mathbf{I}$). Here, $\boldsymbol{\mathcal{A}}_n^{-1} = \boldsymbol{\mathcal{A}}_n^H$ and $\boldsymbol{\mathcal{A}}_n^{-1} \boldsymbol{\mathcal{R}}_z \boldsymbol{\mathcal{A}}_n^{-H} = \sigma_z^2 \mathbf{I}$ so that (10) and (11) simplify to

$$\boldsymbol{\mathcal{C}}_n^{\text{opt}} = \boldsymbol{\mathcal{W}} \boldsymbol{\mathcal{A}}_n^H \quad \text{with } \boldsymbol{\mathcal{W}} = \boldsymbol{\mathcal{V}}_H \big(\boldsymbol{\mathcal{R}}_H + \sigma_z^2 \mathbf{I} \big)^{-1}.$$

Note that $\boldsymbol{\mathcal{W}}$ no longer depends on the symbol index n. Thus, the processing following the first stage $\boldsymbol{\mathcal{Y}}_n = \boldsymbol{\mathcal{A}}_n^H \boldsymbol{\mathcal{X}}_n$ or $y_{n,k} = x_{n,k}/a_{n,k} = x_{n,k}\, a_{n,k}^*$ (cf. (13), (14)) is given by $\widehat{\mathbf{H}}_{n+1} = \boldsymbol{\mathcal{W}} \boldsymbol{\mathcal{Y}}_n$ (cf. (12)). $\boldsymbol{\mathcal{W}}$ corresponds to a *time-invariant* MIMO system that can be precomputed using a *single* matrix inversion. Because $\boldsymbol{\mathcal{R}}_H + \sigma_z^2 \mathbf{I}$ is block-Toeplitz, it can be inverted using the efficient multi-channel Levinson algorithm [15].

5. SIMPLIFIED CHANNEL PREDICTOR

Since the complexity of the full-blown LMMSE predictor is too high, we now develop a simplified predictor that uses a time-invariant MIMO system and FFT techniques.

Time-invariant MIMO system. The first stage of the optimum predictor (see (12)–(14)) is $\boldsymbol{\mathcal{Y}}_n = \boldsymbol{\mathcal{A}}_n^{-1} \boldsymbol{\mathcal{X}}_n$, corresponding to the division $y_{n,k} = x_{n,k}/a_{n,k}$. Assuming that (3) holds exactly, $\mathbf{y}_n$ in (13) and (14) can be expressed as (cf. (8))

$$\mathbf{y}_n = \mathbf{H}_n + \mathbf{u}_n \quad \text{or} \quad y_{n,k} = H_{n,k} + u_{n,k}\,, \tag{15}$$

where $\mathbf{u}_n = [u_{n,0} \cdots u_{n,K-1}]^T$ with $u_{n,k} \triangleq z_{n,k}/a_{n,k}$. Thus, the $y_{n,k}$ equal the true channel weights $H_{n,k}$ up to noise.

We now propose a simplified predictor that consists of the first stage of the LMMSE predictor mentioned above, followed by a *time-invariant* MIMO system. Time invariance is obtained by assuming *random* symbols $a_{n,k}$ that are statistically independent and identically distributed. With this assumption, $\mathbf{u}_n$ is stationary with $\boldsymbol{\mathcal{R}}_u = \mathrm{E}\{\boldsymbol{\mathcal{A}}_n^{-1} \boldsymbol{\mathcal{R}}_z \boldsymbol{\mathcal{A}}_n^{-H}\} = \beta \mathbf{I}$ where $\beta = \sigma_z^2\, \mathrm{E}\{1/|a_{n,k}|^2\}$ (note that the $z_{n,k}$ are *not* assumed uncorrelated). Since also $\mathbf{H}_n$ is stationary, $\mathbf{y}_n = \mathbf{H}_n + \mathbf{u}_n$ in (15) is stationary as well. We now consider LMMSE estimation of $\mathbf{H}_{n+1}$ from the stationary process $\mathbf{y}_n$ (cf. (12)). Using a similar derivation as in Section 4, the coefficient matrix of the LMMSE estimator is obtained as

$$\boldsymbol{\mathcal{W}} = [\mathbf{W}_0 \cdots \mathbf{W}_{L-1}] = \boldsymbol{\mathcal{V}}_H \big(\boldsymbol{\mathcal{R}}_H + \beta \mathbf{I} \big)^{-1}. \tag{16}$$

(Although this is LMMSE-optimum, we suppress the superscript $^{\text{opt}}$ for convenience.) This matrix is *time-invariant*; it can again be precomputed using the multi-channel Levinson algorithm. Note that, formally, (16) is (11) with $\boldsymbol{\mathcal{A}}_n^{-1} \boldsymbol{\mathcal{R}}_z \boldsymbol{\mathcal{A}}_n^{-H}$ replaced by $\mathrm{E}\{\boldsymbol{\mathcal{A}}_n^{-1} \boldsymbol{\mathcal{R}}_z \boldsymbol{\mathcal{A}}_n^{-H}\} = \beta \mathbf{I}$ (cf. [8]).

A simplification can be obtained by constraining the coefficient matrices $\mathbf{W}_m$ to have *band structure*, i.e., only correlations of neighboring subcarriers are exploited for prediction.

DFT-based predictor. For large dimension K, the Toeplitz matrices $\mathbf{R}_H[m]$ involved in (16) are approximately *circulant*. The fact that circulant matrices are diagonalized by the DFT motivates the use of efficient DFT/FFT techniques. In order to obtain a DFT/FFT implementation, we constrain the matrices $\mathbf{W}_m$ to be circulant. Denoting the first column elements of $\mathbf{W}_m$ as $W_0^{(m)}, \ldots, W_{K-1}^{(m)}$, Eq. (12) can be written elementwise as

$$\widehat{H}_{n+1,k} = \sum_{m=0}^{L-1} \sum_{l=0}^{K-1} W_l^{(m)}\, y_{n-m,(k-l) \bmod K}\,.$$

Taking the inverse DFT with respect to k yields

$$\hat{h}_{n+1,m'} = \sum_{m=0}^{L-1} w_{m'}^{(m)}\, \tilde{y}_{n-m,m'} = \mathbf{w}_{m'}^T \tilde{\mathbf{y}}_{n,m'}\,, \quad m' = 0, \ldots, K-1\,, \tag{17}$$

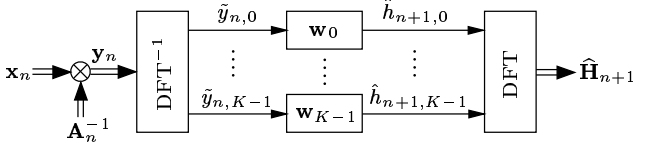

Figure 3: *Efficient DFT/FFT-based channel predictor.*

where $\hat{h}_{n,m'} = \mathrm{DFT}^{-1}_{k\to m'}\{\widehat{H}_{n,k}\} \triangleq \frac{1}{K}\sum_{k=0}^{K-1} \widehat{H}_{n,k}\, e^{j2\pi\frac{km'}{K}}$, $w^{(m)}_{m'} = K\,\mathrm{DFT}^{-1}_{k\to m'}\{W^{(m)}_k\}$, $\tilde{y}_{n,m'} = \mathrm{DFT}^{-1}_{k\to m'}\{y_{n,k}\}$, $\mathbf{w}_{m'} = [w^{(0)}_{m'} \cdots w^{(L-1)}_{m'}]^T$, and $\tilde{\mathbf{y}}_{n,m'} = [\tilde{y}_{n,m'} \cdots \tilde{y}_{n-L+1,m'}]^T$. Since the inverse DFT maps the time/frequency domain to the time/time-lag domain, m' can be interpreted as a tap index. With (15), we obtain

$$\tilde{\mathbf{y}}_{n,m'} = \mathbf{h}_{n,m'} + \tilde{\mathbf{u}}_{n,m'}\,, \tag{18}$$

where $\mathbf{h}_{n,m'} = [h_{n,m'} \cdots h_{n-L+1,m'}]^T$ with $h_{n,m'} = \mathrm{DFT}^{-1}_{k\to m'}\{H_{n,k}\}$ and $\tilde{\mathbf{u}}_{n,m'} = [\tilde{u}_{n,m'} \cdots \tilde{u}_{n-L+1,m'}]^T$ with $\tilde{u}_{n,m'} = \mathrm{DFT}^{-1}_{k\to m'}\{u_{n,k}\}$. There is $\mathrm{E}\{\tilde{\mathbf{u}}_{n,m'}\tilde{\mathbf{u}}^H_{n,m'}\} = \eta\mathbf{I}$ with $\eta = \beta/K$.

Eq. (17) corresponds to the efficient DFT/FFT-based implementation shown in Fig. 3. The diagonalization produced by the inverse DFT allows *separate* calculation of the estimates $\hat{h}_{n+1,m'}$ by means of associated FIR filters $\mathbf{w}_{m'}$ ($m' = 0,\ldots,K-1$).

We will now calculate the LMMSE-optimum filters $\mathbf{w}_{m'}$. It can be shown that the MSE, $\epsilon = \frac{1}{K}\mathrm{E}\{\|\mathbf{e}_{n+1}\|^2\}$ with $\mathbf{e}_{n+1} = \mathbf{H}_{n+1} - \widehat{\mathbf{H}}_{n+1}$, can be written as

$$\epsilon = \sum_{m'=0}^{K-1} \mathrm{E}\{|\tilde{e}_{n+1,m'}|^2\}\,,$$

with $\tilde{e}_{n+1,m'} \triangleq h_{n+1,m'} - \hat{h}_{n+1,m'}$. Since the filtering in (17) is done separately for each m', the individual MSE contributions $\mathrm{E}\{|\tilde{e}_{n+1,m'}|^2\}$ can be minimized separately. Using the orthogonality principle [14], $\mathrm{E}\{\tilde{e}_{n+1,m'}\tilde{\mathbf{y}}^H_{n,m'}\} = \mathbf{0}$, as well as (18) and $\mathrm{E}\{\tilde{\mathbf{u}}_{n,m'}\tilde{\mathbf{u}}^H_{n,m'}\} = \eta\mathbf{I}$ yields the following equations for the optimum coefficients:

$$\mathbf{w}^T_{m'}\big(\mathbf{R}_h[m'] + \eta\mathbf{I}\big) = \mathbf{v}^H_h[m']\,, \quad m' = 0,\ldots,K-1, \tag{19}$$

with the correlations $\mathbf{R}_h[m'] \triangleq \mathrm{E}\{\mathbf{h}_{n,m'}\mathbf{h}^H_{n,m'}\}$ and $\mathbf{v}_h[m'] \triangleq \mathrm{E}\{\mathbf{h}_{n,m'}h^*_{n+1,m'}\}$. We note that the elements of $\mathbf{R}_h[m']$ and $\mathbf{v}_h[m']$ are related to $R_H[m,l]$ in (5) according to

$$\mathrm{E}\{h_{n,m'}h^*_{n-m,m'}\} = \frac{1}{K^2}\sum_{k=0}^{K-1}\sum_{l=0}^{K-1} R_H[m,k-l]\, e^{j2\pi\frac{(k-l)m'}{K}}.$$

The solution of (19) is given by

$$\mathbf{w}^T_{m'} = \mathbf{v}^H_h[m']\big(\mathbf{R}_h[m'] + \eta\mathbf{I}\big)^{-1}, \quad m' = 0,\ldots,K-1.$$

The $L\times L$ matrices $\mathbf{R}_h[m'] + \eta\mathbf{I}$ have Toeplitz structure and thus can be efficiently inverted using the Levinson algorithm [15]. The minimum MSE (MMSE) achieved with the optimum coefficients $\mathbf{w}_{m'}$ can be shown to equal

$$\epsilon_{\min} = R_H[0,0] - \sum_{m'=0}^{K-1} \mathbf{w}^T_{m'}\mathbf{v}_h[m']. \tag{20}$$

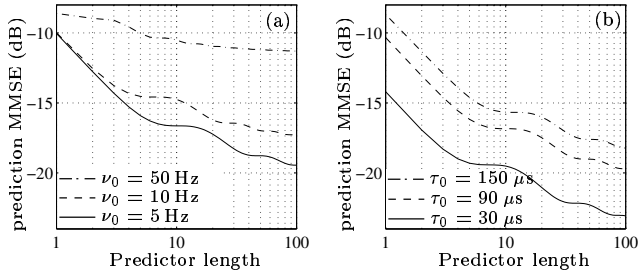

Figure 4: *Prediction MMSE versus predictor length L for* SNR $= 0$ *dB and (a) fixed* $\tau_0 = 100\,\mu s$*, (b) fixed* $\nu_0 = 5$ *Hz.*

Finally, we note that typically $h_{n,m'} \approx 0$ for $m' \geq M$ where the effective maximum delay satisfies $M \ll K$. This implies $\mathbf{v}_h[m'] \approx 0$ for $m' \geq M$ and finally $\mathbf{w}_{m'} \approx 0$ for $m' \geq M$. Thus, computational complexity is further reduced.

6. SIMULATION RESULTS

We studied the performance of the proposed receiver using the DFT-based channel predictor of Section 5. We simulated a conventional OFDM system with $K = 128$ subcarriers, rectangular transmit and receive filters, symbol duration $T = 1.15$ ms, cyclic prefix duration $T_{\mathrm{CP}} = 150\,\mu$s, and subcarrier spacing $F = 1$ kHz. In each symbol interval, a block of 256 bits (obtained by applying a BCH code of length 255 to 131 uncoded bits and adding an additional bit) was mapped to 128 4-PSK symbols $a_{n,k}$ with $|a_{n,k}| = 1$.

The scattering function (see (6)) of the simulated channel was chosen as $S_{\mathbb{H}}(\tau,\nu) = A$ for $0 \leq \tau \leq \tau_0$, $|\nu| \leq \nu_0$ and $S_{\mathbb{H}}(\tau,\nu) = 0$ otherwise. The maximum delay satisfied $\tau_0 < T_{\mathrm{CP}}$. We note that the path loss of the channel is given by $R_H[0,0] \approx R_{\mathbb{H}}(0,0) = 2A\,\tau_0\,\nu_0$. The path loss is relevant to the signal-to-noise ratio SNR $\triangleq R_H[0,0]/\sigma_z^2$ (cf. (3)).

Prediction MMSE. Fig. 4 shows the dependence of the prediction MMSE in (20) on the predictor length L for various τ_0 and ν_0 and an SNR of 0 dB. It is seen that the MMSE decreases with increasing L, which is as expected. Furthermore, for fixed L the MMSE increases with increasing maximum Doppler shift ν_0, which is reasonable since faster channels are more difficult to predict (note, however, that slower channels typically require a larger predictor length to exploit all available correlations). Finally, for fixed L the MMSE also increases with increasing maximum delay τ_0. Indeed, a larger τ_0 implies a smaller coherence bandwidth of the channel [10], i.e., less spectral correlation of the time-varying transfer function that can be exploited by the predictor.

Receiver performance. Next, we simulated the proposed receiver using the DFT-based channel predictor of Section 5. The results shown in Fig. 5 were obtained from 10^4 Monte Carlo runs. There occurred error propagation due to decision-directed operation (only 10 training symbol intervals were used for predictor initialization). Parts (a)–(c) of Fig. 5 show the prediction MSE, symbol MSE $\mathrm{E}\{|\alpha_{n,k} - a_{n,k}|^2\}$, and bit error rate (BER), respectively, for a channel with $\tau_0 = 150\,\mu$s and $\nu_0 = 10$ Hz. Parts (d)–(f) of Fig. 5 show the same for a faster channel with $\tau_0 = 150\,\mu$s and $\nu_0 = 50$ Hz.

Fig. 5(a) compares the theoretical prediction MMSE in (20), the measured prediction MSE obtained with our channel pre-

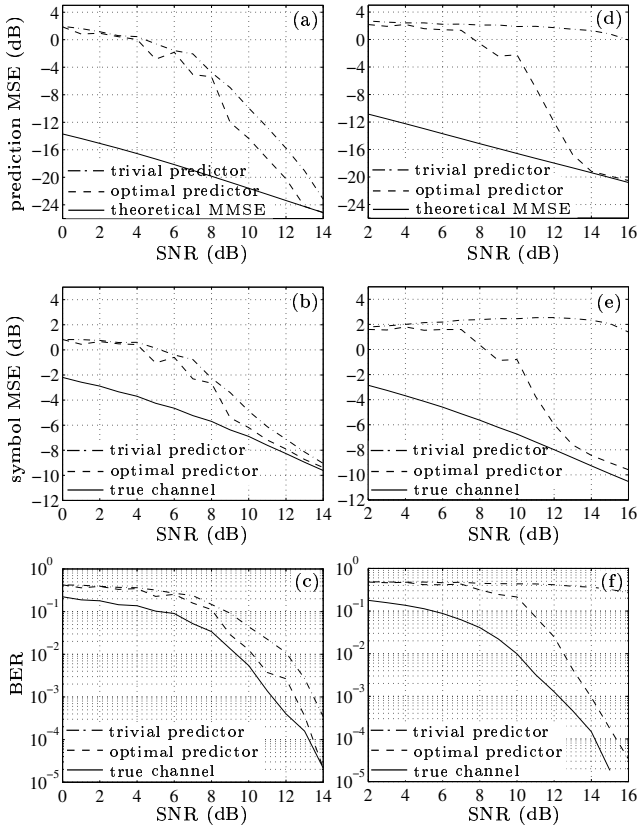

Figure 5: *Performance of a coded OFDM system with predictive equalization: (a) prediction MSE, (b) symbol MSE, and (c) bit error rate for a "slow" channel ($\nu_0 = 10\,Hz$); (d)–(f) the same for a "fast" channel ($\nu_0 = 50\,Hz$).*

dictor, and the measured prediction MSE of a trivial predictor reproducing the previous channel estimate [7]. The substantial difference between measured and theoretical results at low SNR is due to error propagation. For reasonable SNR values, our predictor performs significantly better than the trivial predictor. A similar behavior is observed in Figs. 5 (b) and (c). These figures compare the symbol MSE and BER, respectively, obtained using knowlede of the true channel parameters, using our channel predictor, and using the trivial channel predictor.

Finally, parts (d)–(f) show that faster channel variations generally result in poorer performance (this is partly due to ICI resulting from the larger Doppler shifts). However, whereas for reasonable SNR values our predictive equalizer still yields acceptable performance (in particular, its prediction MSE approaches the theoretical optimum for SNR values larger than about 13 dB), the trivial predictor is unable to track the channel variations and its performance remains unacceptable for all SNR values.

7. CONCLUSIONS

We have proposed a receiver for orthogonal/biorthogonal frequency division multiplexing (OFDM/BFDM) communications over random time-varying channels. The novel receiver uses decision-directed predictive equalization and thus does not require regular transmission of pilot symbols. Although certain simplifications and approximations were made for the sake of computational efficiency, numerical simulations showed that for reasonable SNR values the performance of our channel predictor can be nearly optimum.

The design of the channel predictor assumed knowledge of the channel's second-order statistics. For practical implementations, *adaptive* versions of the predictor are advantageous since they do not require this prior knowledge and allow to track time variations of the channel statistics [16].

REFERENCES

[1] R. W. Chang, "Synthesis of band-limited orthogonal signals for multi-channel data transmission," *Bell Syst. Tech. J.*, vol. 45, pp. 1775–1796, Dec. 1966.

[2] S. B. Weinstein and P. M. Ebert, "Data transmission by frequency division multiplexing using the discrete Fourier transform," *IEEE Trans. Comm. Tech.*, vol. 19, pp. 628–634, Oct. 1971.

[3] J. A. C. Bingham, "Multicarrier modulation for data transmission: An idea whose time has come," *IEEE Commun. Mag.*, vol. 28, pp. 5–14, May 1990.

[4] H. Sari, G. Karam, and I. Jeanclaude, "Transmission techniques for digital terrestrial TV broadcasting," *IEEE Communications Magazine*, vol. 33, pp. 100–109, Feb. 1995.

[5] W. Kozek and A. F. Molisch, "Nonorthogonal pulseshapes for multicarrier communications in doubly dispersive channels," *IEEE J. Sel. Areas Comm.*, vol. 16, pp. 1579–1589, Oct. 1998.

[6] H. Bölcskei, "Design of pulse shaping filters for wireless OFDM systems," in *Proc. SPIE Wavelet Applications in Signal and Image Processing III*, (Denver, CO), July 1999.

[7] Y. Li, L. Cimini, and N. Sollenberger, "Robust channel estimation for OFDM systems with rapid dispersive fading channels," *IEEE Trans. Comm.*, vol. 46, pp. 902–915, July 1998.

[8] O. Edfors, M. Sandell, J.-J. van de Beek, S. Wilson, and P. Börjesson, "OFDM channel estimation by singular value decomposition," *IEEE Trans. Comm.*, vol. 46, pp. 931–939, July 1998.

[9] P. A. Bello, "Characterization of randomly time-variant linear channels," *IEEE Trans. Comm. Syst.*, vol. 11, pp. 360–393, 1963.

[10] J. D. Parsons, *The Mobile Radio Propagation Channel*. London: Pentech Press, 1992.

[11] W. Kozek, "On the transfer function calculus for underspread LTV channels," *IEEE Trans. Signal Processing*, vol. 45, pp. 219–223, Jan. 1997.

[12] G. Matz and F. Hlawatsch, "Time-frequency transfer function calculus (symbolic calculus) of linear time-varying systems (linear operators) based on a generalized underspread theory," *J. Math. Phys.*, vol. 39, pp. 4041–4071, Aug. 1998.

[13] H. Artés, G. Matz, and F. Hlawatsch, "Unbiased scattering function estimation during data transmission," in *Proc. IEEE VTC-99 Fall*, (Amsterdam, The Netherlands), pp. 1535–1539, Sept. 1999.

[14] S. M. Kay, *Fundamentals of Statistical Signal Processing: Estimation Theory*. Englewood Cliffs (NJ): Prentice Hall, 1993.

[15] S. M. Kay, *Modern Spectral Estimation*. Englewood Cliffs (NJ): Prentice Hall, 1988.

[16] D. Schafhuber, G. Matz, and F. Hlawatsch, "Equalization in wireless OFDM systems using adaptive channel prediction," in preparation.